Molecular Therapy
Nucleic Acids
Original Article

Enhancing mRNA translation efficiency by introducing sequence optimized AU-rich elements in 3′ UTR via HuR anchorage

Xinghuan Ma,[1] Sujia Liu,[1] Bangda Fan,[1] Danni Jin,[1] Lei Miao,[2,3] Lin Liu,[1] Shubo Du,[1] and Jiaqi Lin[1]

[1]MOE Key Laboratory of Bio-Intelligent Manufacturing, School of Bioengineering, Dalian University of Technology, Dalian 116024, China; [2]State Key Laboratory of Natural and Biomimetic Drugs, School of Pharmaceutical Sciences, Peking University, Beijing 100191, China; [3]Beijing Key Laboratory of Molecular Pharmaceutics, School of Pharmaceutical Sciences, Peking University, Beijing 100191, China

mRNA technology holds immense promise as an innovative therapeutic approach with applications spanning infectious disease vaccines, cancer immunotherapy, protein replacement, and gene editing. However, practical use of mRNA has been hindered by challenges such as low cellular stability and transient protein expression. For addressing these, we propose a novel strategy to optimize mRNA sequences, particularly in the untranslated region, by inserting adenylate/uridylate-rich elements (AU-rich elements) to enhance stability and protein expression. Our investigation revealed that integrating AU-rich elements between the open reading frame (ORF) and the 3′ untranslated region (3′ UTR) significantly enhances RNA stability compared with other insertion sites. We identified cytoplasmic Human antigen R (HuR) as an essential RNA-binding protein responsible for promoting mRNA stability and translation, confirmed through HuR knockdown experiments and pull-down assays between AU-rich elements and HuR. Through rational design, we optimized the sequence of natural AU-rich elements and identified the essential "AUUUA" element, which, with certain repeats, can increase protein expression up to 5-fold. To demonstrate the universality of AU-rich element sequences in enhancing mRNA translation, we switched the coding proteins from luciferase to EGFP, mCherry, and ovalbumin (OVA), finding that both natural and engineered AU-rich element sequences amplify the expression of these proteins. In conclusion, leveraging the functionalities of RNA-binding proteins and the natural regulation of RNA stability in the untranslated region represents a novel strategy to enhance mRNA pharmacokinetics in the cytoplasm, expanding the potential applications of mRNA in therapeutic drugs.

INTRODUCTION

The rapid design and development of two COVID-19 mRNA vaccines marked the advent of a new biotechnology platform for immunization against severe acute respiratory syndrome coronavirus 2 (SARS-CoV-2) and, potentially, a wide spectrum of microbial pathogens and cancers.[1] The remarkably short time frame from target identification to phase 1 clinical studies, along with the convincing safety profile of mRNA vaccines after billions of administered doses, underscores the potential of a new generation of mRNA therapeutics that extends beyond conventional vaccines and other agents relying on the ability of mRNA and lipid nanoparticles (LNPs) to stimulate immune responses.[2] The advantages of mRNA therapy include its high efficiency, good safety profile, and relatively low production costs. As the success of mRNA therapy relies on the efficiency of mRNA translation, optimizing mRNA sequences to maximize intracellular therapeutic protein expression levels is the primary goal.[3]

Effective mRNA design strategies are crucial, and optimizing untranslated regions (UTRs) can improve the bioavailability of encoded proteins.[4,5] Previous research has focused on increasing mRNA stability by using single highly stable UTRs derived from *HBA1* and *HBB* genes or concatenating two copies, which have been demonstrated to enhance translation level and stability.[6] However, the use of globin UTR sequences for construct design has drawbacks, such as restricted translation efficiency due to the presence of a single type of UTR sequence.[7] To address the need for universal design principles to generate stable and highly expressed mRNAs, other researchers have employed high-throughput methodologies to design,[8] screen, and optimize mRNAs with extensive variability in the 5′ UTR, open reading frame (ORF), and 3′ UTR.[9] This approach aims to identify novel UTR sequences and methodically combine 5′ UTR and 3′ UTR to maximize translation efficiency.[10] A rapid method for obtaining ideal mRNA sequences involves constructing machine learning models to process large-scale data. Combining sequence optimization strategies based on codon adaptation index and minimum free energy, algorithms can swiftly generate stable and highly efficient translated mRNA sequences within minutes.[11,12] Additionally, optimizing UTR sequences with high-throughput screening methods resents

Received 23 August 2024; accepted 10 February 2025;
https://doi.org/10.1016/j.omtn.2025.102485.

Correspondence: Shubo Du, MOE Key Laboratory of Bio-Intelligent Manufacturing, School of Bioengineering, Dalian University of Technology, Dalian 116024, China.
E-mail: dushubo@dlut.edu.cn
Correspondence: Jiaqi Lin, MOE Key Laboratory of Bio-Intelligent Manufacturing, School of Bioengineering, Dalian University of Technology, Dalian 116024, China.
E-mail: jqlin@dlut.edu.cn

challenges due to experimental complexity. From a molecular biology perspective, it is difficult to predict complex intracellular translation mechanisms using deep learning algorithms, and the specific molecular mechanisms underlying optimized sequences remain to be fully elucidated. The classic mRNA comprises the ORF, 5′ and 3′ UTR, and a polyadenylated tail. Within cells, the 3′ UTR is a critical factor in regulating mRNA dynamics, as it contains various sequence elements such as microRNA recognition sites, adenylate/uridylate-rich (AU-rich) elements, GU-rich elements, etc. These elements interact with RNA-binding proteins, microRNAs, long non-coding RNAs, and other factors collectively regulate mRNA stability, subcellular localization, and translation efficiency, ultimately affecting protein output.[13,14] Different *cis*-acting factors binding within the 3′ UTR can render mRNA either stable[15–17] or unstable.[18] For instance, within the RNA-binding protein (RBP) family, the Hu family, especially members like Human antigen R (HuR), are known for their stabilizing effects on eukaryotic mRNAs by binding to AU-rich elements in the 3′ UTR contributing to increased stability and longer half-life of the mRNAs.[19,20] Investigations have shown that many viruses and pathogens exploit proteins like members of the Hu and PCBP families to enhance the stability of their RNAs.[21]

In this paper, we propose a new mRNA sequence optimization method by rational design, focusing on the interaction of molecular pairs involving HuR and AU-rich elements into sequence design. HuR, an RNA-binding protein, which widely presents in mammalian cytoplasm, can anchor AU-rich elements and bind to the 3′ UTR in a sequence-specific manner, thereby regulating RNA stability and protein expression. Simultaneously, we iteratively optimize AU-rich elements, extensively studying the shortest core sequences and optimal repeat lengths that ensure translation enhancement and validating them both *in vitro* and *in vivo*. Moreover, our data demonstrate the necessity of HuR binding for stabilizing mRNA targets containing AU-rich elements. Overall, our research proves the feasibility of this novel sequence optimization approach, providing an interesting exploration case for optimizing mRNA's 3′ UTR sequences with RNA-binding proteins.

RESULTS

Inserting AU-rich elements into the 3′ UTR of mRNA can enhance mRNA stability and translation

The 3′ UTR is a crucial component of mRNA sequence optimization, which can influence mRNA stability and spatially correct translation. To examine the effects of inserting AU-rich elements into the 3′ UTR and the insertion site of element on mRNA stability and translation, we designed and synthesized four sequences of firefly luciferase RNA (Figure 1A), with all sequences being identical except for the 3′ UTR (Table S1). The AU-rich element was a 50-nucleotide (nt) AT sequence from a human lymphokine gene, granulocyte-macrophage colony-stimulating factor (*GM-CSF*).[22] A control group (Non-ARE) was established employing conventional structured RNA without AU-rich element insertion in the 3′ UTR (295 nt) of firefly luciferase, while the other three mRNAs each incorporated an AU-rich element at the beginning (ARE-F), middle (ARE-M), and end (ARE-R) of the 3′ UTR sequence, respectively. The conventional structured RNA includes a 5′ UTR derived from human α-globin, a 3′ UTR composed of a combination of human mitochondrial 12S rRNA and human *AES/TLE5* gene, along with a poly A tail. These sequences are identical to those used in the SARS-CoV-2 mRNA vaccine BNT162b2, as previously published,[23,24] to maintain translation efficiency and intracellular stability. Cellular luciferase expression levels were used to represent the translation efficiency of RNA. Analysis of relative luciferase expression levels 24 h after mRNA transfection revealed varying degrees of enhancement in luciferase expression for ARE-F, ARE-M, and ARE-E compared with Non-ARE. Among these three insertion positions, inserting AU-rich elements at the front of the UTR sequence (ARE-F) yielded the most significant enhancement, with the highest expression of luciferase (Figure 1B) and RNA abundance observed (Figure S2A). To verify whether the enhanced translation effect of AU-rich elements depended on specific cell types, we conducted validations in different cell lines, including human cancer cells HeLa and A549, normal human cells HEK-293T, DC model cells DC2.4, and murine cancer cells 4T1. While the degree of enhancement varied among the five different cell lines, the trend was consistent, with ARE-F showing the most significant relative enhancement in luciferase expression, while ARE-M and ARE-R exhibited only slight enhancements in translation efficiency. These data implicated that addition of the AU-rich element was a contributing factor toward the protein expression enhancement effect.

To thoroughly investigate the effect of AU-rich element insertion on mRNA stability and translation, the relative luciferase expression level and mRNA abundance were analyzed based on raw and normalized signals. Luciferase expression levels were detected at 6, 12, 24, and 48 h after transfection of ARE-F and Non-ARE mRNA. Results showed a significant increase in both protein expression and mRNA abundance of ARE-F compared with Non-ARE within the observed four time points (Figures 1C and 1D). The relative luciferase expressions of ARE-F at 24 h post-transfection, corresponding to the peak mRNA expression, showed an approximately 3-fold increase compared with Non-ARE (Figure 1C). Both Non-ARE and ARE-F luciferase expression gradually increased within the first 12 h after transfection. Non-ARE expression peaked at 12 h and subsequently declined, while ARE-F attained its maximal level at 24 h post-transfection. As protein expression levels are directly correlated with mRNA stability, we measured luciferase mRNA abundance by qPCR at different time points post-transfection. As shown in Figures 1D and 1E, during the 48-h detection period post-transfection, the cytoplasmic RNA abundance of ARE-F remained consistently higher than that of Non-ARE. By the 48 h post-transfection mark, the cytoplasmic mRNA abundance of ARE-F was 4.8 times higher than that of Non-ARE. Therefore, the data above suggest that protein expression is positively correlated with RNA stability. The insertion of AU-rich elements enhances RNA stability, which, in turn, promotes improved RNA translation.

Next, we evaluated the effect of inserting AU-rich elements within the 3′ UTR *in vivo*. A lipid-nanoparticle material specialized for mRNA vaccine delivery was used to deliver ARE-F and Non-ARE mRNAs in mice. Vaccines were administered via subcutaneous injection to

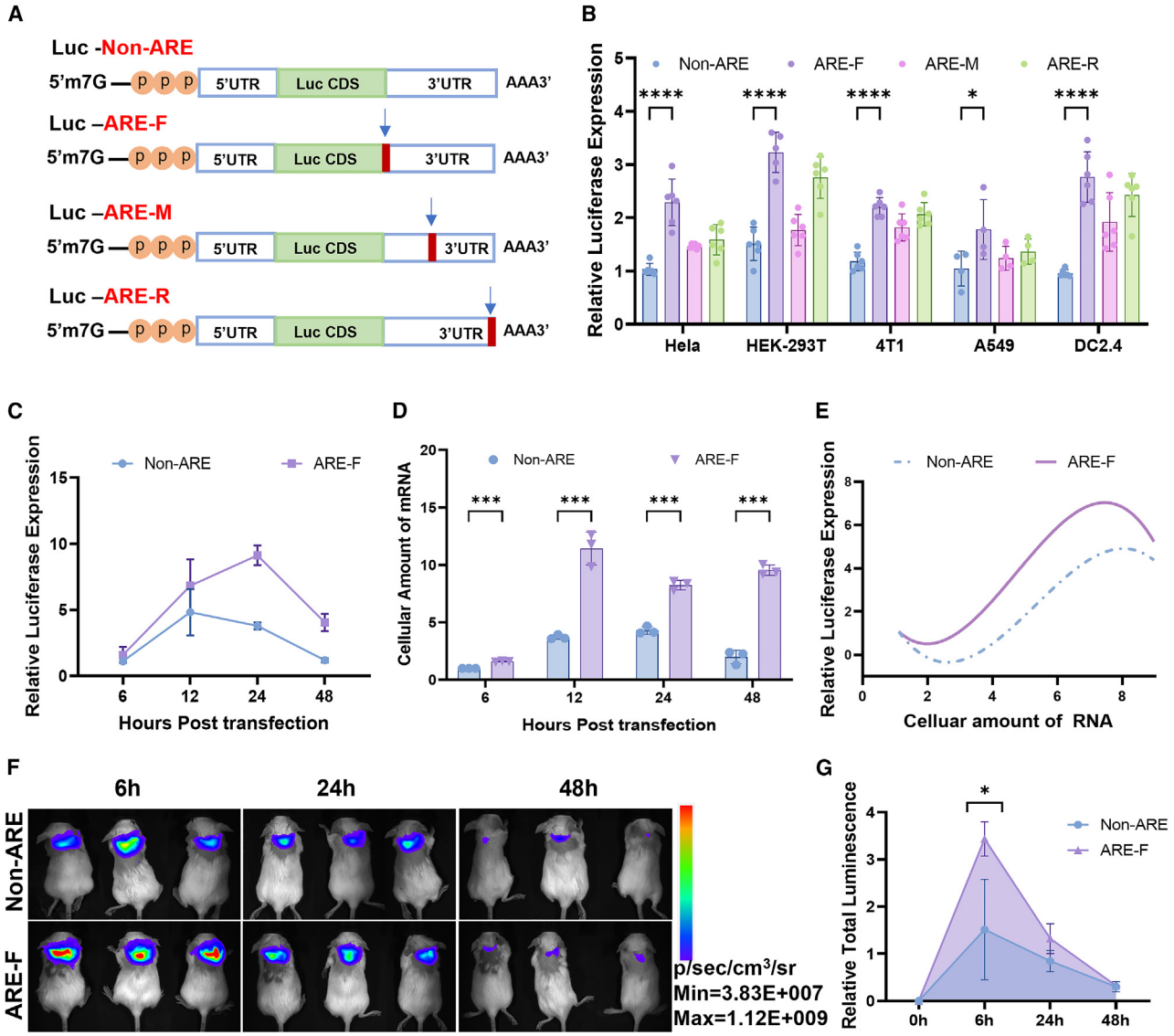

Figure 1. Enhancement of intracellular mRNA abundance and protein expression by insertion of AU-rich elements in the 3′ UTR

(A) Schematic representation of three different positions of AU-rich element insertion in the 3′ UTR. (B) Relative luciferase expression of ARE-F, ARE-M, and ARE-R in different cells 24 h post-transfection. $n = 6$. (C) Relative protein expression of ARE-F and Non-ARE at 6, 12, 24, and 48 h post-transfection. $n = 3$. (D) qPCR detection of cellular abundance at different time points post-transfection of ARE-F and Non-ARE. $n = 3$. (E) The ratio of luciferase expression to RNA levels, highlighting the relationship between RNA stability and translation efficiency. (F) *In vivo* validation of protein expression of ARE-F and Non-ARE in mice. (G) Relative total luminescence intensity at different time points after injection of luciferase RNA in mice. $n = 3$. Data are presented as mean ± SD. Student's t test was used to evaluate significant differences: * $p < 0.05$, * * $p < 0.01$, * * * $p < 0.001$; NS, not significant.

the mice. The production of luciferase was observed *in vivo* at 6, 24, and 48 h using live imaging. The results indicated that following mRNA injection, protein expression peaked for both ARE-F and Non-ARE at 6 h and then declined at 24 and 48 h post-injection (Figure 1G). Figures 1F and 1G show that mice injected with ARE-F consistently exhibited stronger bioluminescent signals at all three time points. Importantly, the bioluminescence produced by ARE-F at 24 h was comparable to the bioluminescence of Non-ARE mRNA at 6 h. This agrees with the *in vitro* findings for ARE-F, indicating that mRNA containing AU-rich elements can extend the window of high protein production and the overall duration of protein synthesis.

Binding HuR by ARE is necessary for the enhanced translation of mRNA

To assess the role of HuR in enhancing ARE-F mRNA translation, we evaluated the levels of luciferase protein expression and mRNA

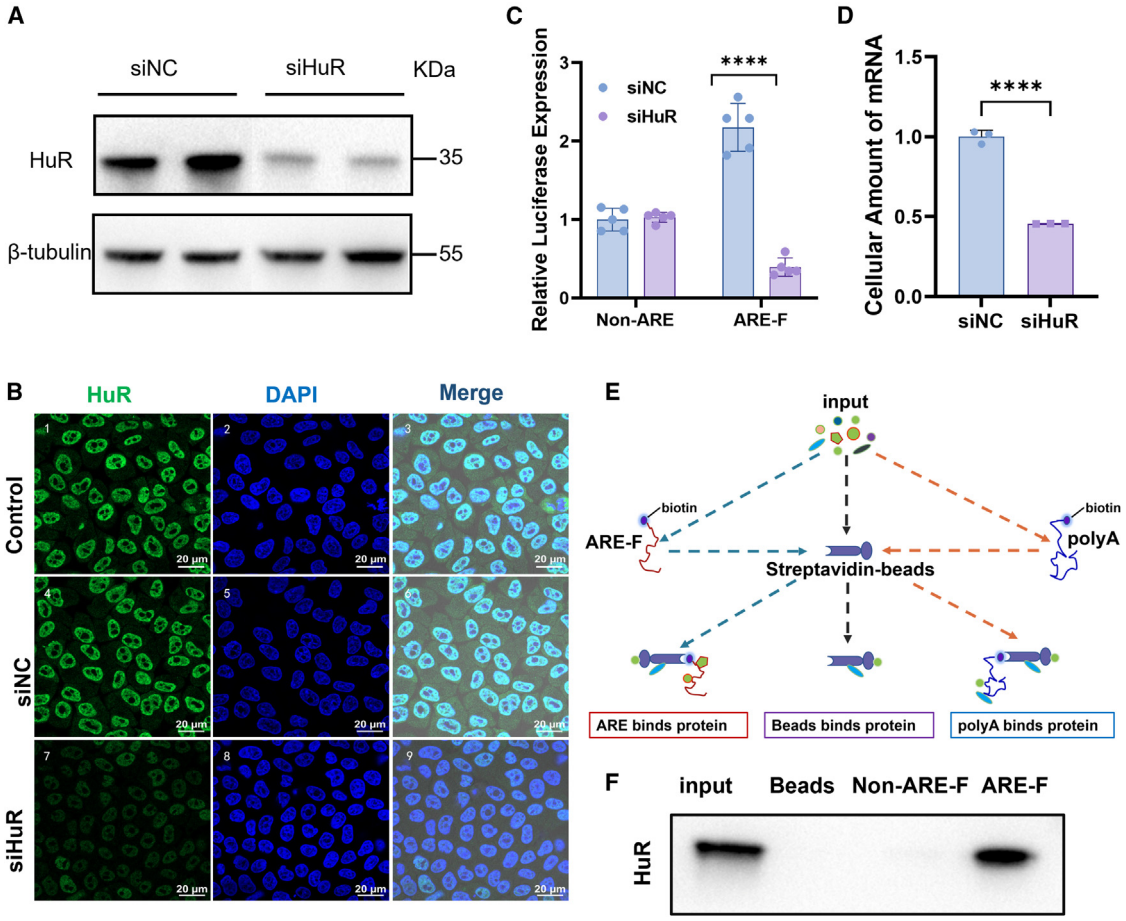

Figure 2. Decrease in protein expression and cellular abundance of ARE-F after HuR silencing

(A) Western blot analysis of HuR expression before and after siRNA-mediated silencing in cells. (B) Immunofluorescence detection of changes in HuR before and after siRNA-mediated silencing in cells. (C) Cellular protein expression of ARE-F and Non-ARE after siRNA-mediated HuR silencing. $n = 6$. (D) Changes in RNA abundance of ARE-F and Non-ARE after siRNA-mediated HuR silencing. $n = 3$. (E) Schematic representation of RNA pull-down technique. (F) Identification of ARE-F and HuR binding using RNA pull-down assay. Data are presented as mean ± SD.Student's t test was used to evaluate significant differences: * $p < 0.05$, * * $p < 0.01$, * * * $p < 0.001$; NS, not significant.

abundance in cells in response to changes in HuR protein level. Initially, we transfected HuR small interfering RNA (siRNA) to silence the expression of HuR protein in HeLa cells, which resulted in around 60% reduction of intracellular HuR protein compared with control siRNA transfection (Figure 2A). Immunofluorescence displayed that HuR mainly localizes in the nucleus and shuttles between the nucleus and the cytoplasm, which also revealed a discernible decrease in the fluorescence intensity corresponding to HuR protein following transfection with HuR siRNA (Figure 2B). In the cellular environment with reduced levels of HuR protein through RNAi, we transfected Non-ARE and ARE-F mRNA. Significantly, when the cytoplasmic HuR protein was reduced, the enhanced effect of ARE-F sharply decreased, resulting in a notable decrease in luciferase expression. However, the variations in HuR protein levels had no impact on Non-ARE expression (Figure 2C). We further investigated if silencing HuR affects the intracellular RNA abundance of ARE-F. Through qRT-PCR analysis, an approximate 60% decrease in ARE-F RNA levels was observed post-HuR silencing compared with the siNC control group (Figure 2D), consistent with the reduction in HuR protein abundance.

The RNA pull-down technique has been widely used to investigate interactions between RNA and proteins. RNA-binding proteins play crucial roles in gene expression regulation by influencing mRNA stability and translation efficiency. We synthesized a biotinylated ARE-F probe and a Non-ARE-F probe as a control. To match the length of the ARE-F probe, the Non-ARE-F probe was a biotinylated polyA RNA probe that was unrelated to HuR protein to capture protein-RNA complexes of interest, along with unbound streptavidin magnetic beads as a negative control. The RNA probes and HeLa cell lysate were incubated to allow the *in vitro* interaction to occur, and the fraction of bound protein was analyzed through western blotting (Figure 2E). As shown in Figure 2F, HuR protein bands that appeared at 35 kDa were only observed in the input group and the ARE-F

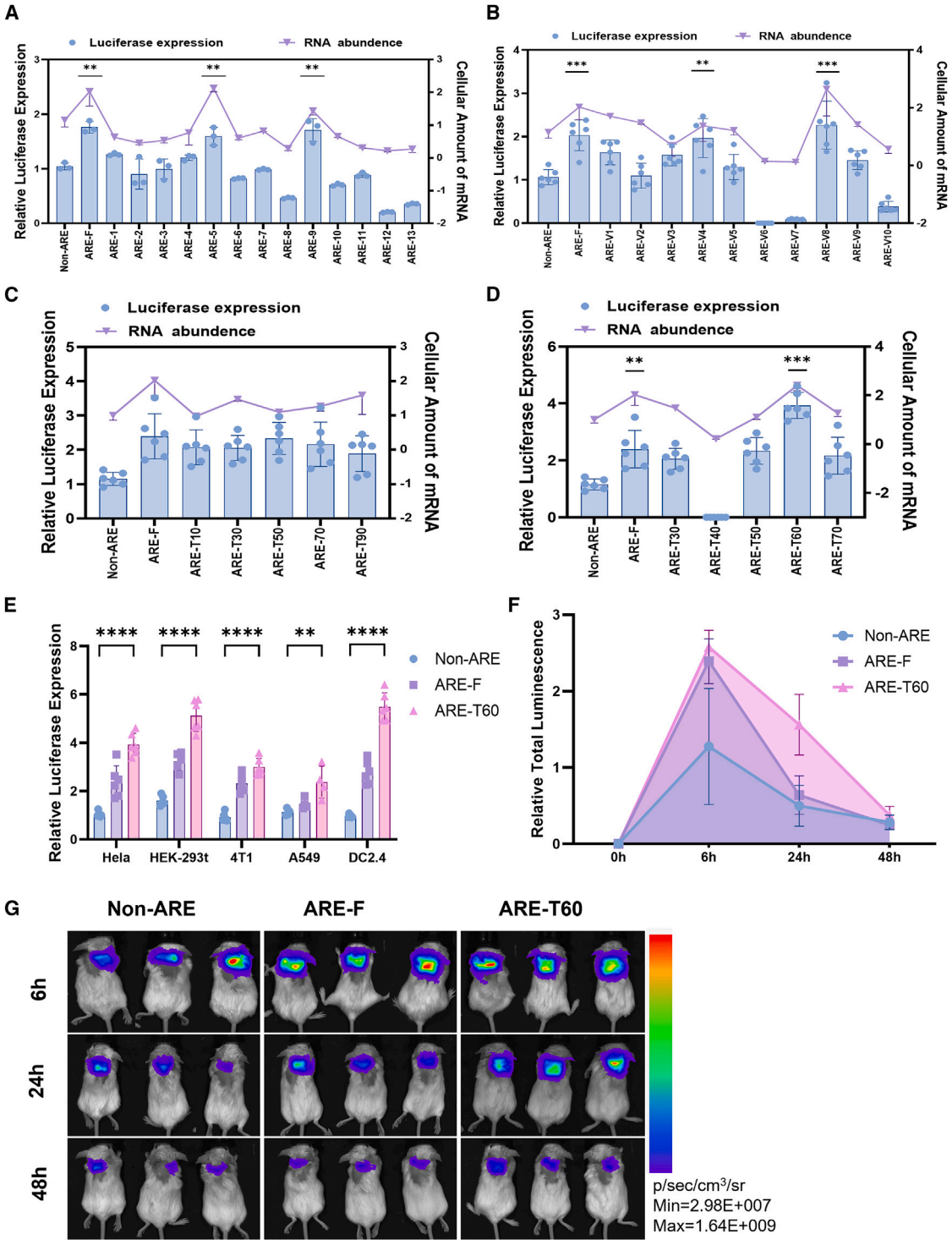

Figure 3. Exploration of sequence patterns for enhancing translation efficiency of AU-rich elements

(A) Relative luciferase expression levels and RNA abundance of randomly selected AU-rich element mRNAs from a natural gene library. $n = 3$. (B) Relative luciferase expression levels and RNA abundance 24 h post-transfection of cells with mRNA constructs containing truncated ARE-F elements (AREV1-V10). $n = 6$. (C) Relative luciferase expression levels and RNA abundance 24 h post-transfection of cells with mRNA constructs containing five copies of AUUUA with a 20-bp spacing interval (ARET10-T90).

(legend continued on next page)

group, poly(A) binding protein (PABP) was also analyzed by western blot as a control protein for HuR, ARE-F was undetectable at the size of PABP (Figure S1). In summary, through the RNA pull-down experiment, we directly identified cofactors that bind to ARE-F, demonstrating that the binding of the RNA-binding protein HuR with the ARE-F element is essential for the enhanced effect of ARE-F.

Rational design of the natural AU-rich elements

To explore the sequence regulatory rule that enhances mRNA translation of AU-rich elements and further optimize the sequences, we attempted to identify some patterns from a natural gene library. Thus, we selected 13 different sequences of AU-rich elements from oncogenes, cytokines, or transcription factors, because AU-rich elements are predominantly present in the 3′ UTR of these genes (Table S2). We inserted these 13 types of AU-rich elements in front of the 3′ UTR in a manner similar to ARE-F and named them ARE1–13 sequentially (Table S3). We sought to quantify the activity of these AU-rich elements at the translation level. As shown in Figure 3A, the composition of different AU-rich elements significantly influenced mRNA translation. Among them, two sequences, ARE-5 and ARE-9, demonstrated significantly higher luciferase protein expression compared with Non-ARE, exhibiting translation enhancement capabilities similar to ARE-F, while the other substitutions in the UTR either exhibited little effect or caused reduction in protein production, The trend of RNA abundance and protein expression within the cells is consistent, with the RNA abundance of ARE-5 and ARE-9 being significantly higher than that of Non-ARE (Figure 3A). By analyzing the enhancing sequences ARE-F, ARE-5, and ARE-9, we found that these sequences all contained repeating AUUUA sequences, with ARE-F exhibiting the highest number of AUUUA repeats. Therefore, we decided to further investigate the role of AU-rich elements starting from the enhancing sequences of ARE-F.

First, the AU-rich sequence length of ARE-F is 50 nt. We sequentially truncated the ARE-F sequence, deleting irrelevant parts to explore the shortest functional sequence for enhancing translation. Based on ARE-F, we progressively shortened the AU-rich element in a binary fashion, performing a total of three truncations, generating six truncated sequences, namely AREV1–V6 (Table 1). The expression of luciferase post-transfection is depicted in Figure 3B. ARE-V4 displayed protein expression enhancement comparable to ARE-F, with the AU-rich functional sequence being reduced from 50 nt to 12 nt. By observing the sequence composition, we noticed that the AU-rich element of ARE-V4 exhibited a distinct pattern, consisting of two repeats of AUUUA and a consecutive uridine extension arm. Building upon the pattern found from ARE-V4, we designed six sequences, AREV5–V10, featuring different positions and quantities of uridine extension arms based on the two AUUUA repeats. This exploration aimed to further investigate the precise binding sequence crucial for maintaining the enhancing effect, as well as the function of the uridine extension arms on both sides in the enhancing effect. Surprisingly, when all uridine extension arms were removed, namely ARE-V8, it not only exhibited the translation enhancement effect of ARE-F but also possessed the simplest AU-rich sequence, composed of only two repeated AUUUA sequences. In accordance with the elevated levels of translated protein expression, the RNA abundance of ARE-V8 also exhibited increased levels (Figure 3B). Therefore, the shortest functional sequence for HuR binding to AU-rich elements, enhancing RNA stability and protein expression, is 9 nt, specifically AUUUAUUUA.

Based on the observation that the shortest functional AU-rich element consists of two AUUUA repeats, we aimed to explore the optimal length of AUUUA repeat sequences for AU-rich element functionality. Therefore, we conducted a series of mutations in AU-rich elements to assess the impact of AUUUA repeat count on protein yield (Table 2). Following the length of repeats in AU-rich elements as the design principle, we designed a total of five new AU-rich elements, all constructed by linking AUUUA repeats. These repeat lengths ranged from 10 to 90 nt with intervals of 20 nt between sequences and were named ARET10–T90. After transfection, the luciferase expression correlated with the number of AUUUA repeats, reaching its peak at a length of 50 nt (Figure 3C). Therefore, near the 50-nt mark, we designed two sequences at intervals of 10 nt, measuring 40 nt and 60 nt, named T40 and T60. Post-transfection of cells revealed that, compared with Non-ARE, ARE-F exhibited significantly enhanced translation effects consistent with previous observations. Surprisingly, ARE-T60 significantly enhanced translation beyond ARE-F, showing a significant increase in protein expression at 60 nt (Figure 3D). In terms of enhanced translation levels, the order of translation enhancement was ARE-T60 > ARE-F > Non-ARE. The stability of intracellular RNA was analyzed with qPCR, the highest abundance of intracellular RNA was observed at ARE-T60 (Figure 3D). Therefore, within the range of 10–90 nt, AU-rich elements exhibited the optimal translation enhancement effect with a length of 60 nt. In addition, to investigate whether modified nucleotides and different UTRs impact the AU-rich enhancer, *in vitro* transcription was performed using unmodified UTP. We found that both ARE-F and ARE-T60 could enhance protein expression with both N1-Me pseudo-UTP and unmodified UTP (Figure S3A). Furthermore, we replaced the 3′ UTR with that of β-globin, which, consistent with the results from BNT162b2, demonstrated that ARE-T60 could significantly enhance protein expression by approximately 4-fold (Figure S3B).

$n = 6$. (D) Relative luciferase expression levels and RNA abundance 24 h post-transfection of cells with mRNA constructs containing five copies of AUUUA with a 10-bp spacing interval near the peak of ARE-T50 (ARET30-T70). $n = 6$. (E) Sequential enhancement effects of Non-ARE, ARE-F, and ARE-T60 validated in different cells. $n = 6$. (F) Relative fluorescence signal intensity of mice injected with Non-ARE, ARE-F, and ARE-T60 mRNA. $n = 3$. (G) Real-time imaging of mice at 6 h, 24 h, and 48 h post-injection of Non-ARE, ARE-F, and ARE-T60 mRNA. Data are presented as mean ± SD. Student's t test was used to evaluate significant differences: * $p < 0.05$, * * $p < 0.01$, * * * $p < 0.001$; NS, not significant.

Table 1. AU-rich element sequences of AREV1–V6

Serial number	AU-rich sequence
ARE-V1	TAATATTTATATATTTATATTTTTA
ARE-V2	AAATATTTATTTATTTATTTATTTA
ARE-V3	AAATATTTATTTA
ARE-V4	TTTATTTATTTA
ARE-V5	TAATATTTATATA
ARE-V6	TTTATATTTTTA
ARE-V7	TATTTATTTA
ARE-V8	ATTTATTTA
ARE-V9	ATTTATTTATTT
ARE-V10	TTTATTTATTTATTT

Finally, we validated the enhanced effects of the progressively optimized ARE-F and ARE-T60 both *in vitro* and *in vivo*. We transfected the two rounds of optimized sequences into different types of cells, with the results shown in Figure 3E. Compared with Non-ARE, it can be observed that in each type of cell, ARE-F and ARE-T60 both demonstrated progressively enhanced translation effects. In DC2.4, the protein expression of ARE-T60 after sequence optimization increased by about six times compared with Non-ARE. In the *in vivo* validation, we delivered equal amounts of Non-ARE, ARE-F, and ARE-T60 into mice using lipid nanoparticles and measured the expression of luciferase in mice at the 6th, 24th, and 48th hours. The characterization of lipid nanoparticles is shown in Figure S4. The RNA encapsulation efficiency is approximately 80%–90%. Dynamic light scattering (DLS) measurements revealed that the hydrodynamic diameters of the lipid nanoparticles range from 110 to 130 nm, with a narrow size distribution. According to Figures 3F and 3G, at 6 h, the mRNA from three types of injections reached peak luciferase expression. Over three observation time points, the increase in intracellular luciferase expression remained consistent with the mRNA optimization sequence, indicating consistent expression trends of the optimized sequences both *in vitro* and *in vivo*. In conclusion, the enhancing effect of AU-rich elements is correlated with the length of the sequence composition.

The engineered AU-rich elements can serve as a universal translation enhancing tool

To demonstrate the potential therapeutic utility of these optimized AU-rich elements, we sought to utilize them as a sequence optimization tool to enhance the expression of various proteins. Previous studies have utilized luciferase as an indicator of mRNA sequence expression efficiency, but this method relies on indirect measurement of the chemiluminescent reaction product catalyzed. In contrast, fluorescent proteins may be a preferable option as they can directly reflect protein expression levels through fluorescence intensity.

Utilizing this efficient system, as shown in Figures 4A and S5A, we constructed EGFP-ARE-F, EGFP-ARE-T60, mCherry-ARE-F, and mCherry-ARE-T60. These constructions were sequentially optimized using AU-rich elements from ARE-F and ARE-T60, with EGFP original and mCherry original serving as controls. The expressed proteins in the cells were qualitatively and quantitatively analyzed 24 h after transfection. AS showed in Figure 4B, the results of a confocal laser scanning microscopy (CLSM) experiment demonstrated a sequential increase in fluorescence intensity for EGFP-ARE-F and EGFP-ARE-T60, in contrast to the EGFP control group, with mCherry exhibiting a similar trend. As illustrated in Figures 4C and S5B, qualitative analysis of flow cytometry showed an increase in protein expression in turn. Collectively, these two sets provide compelling evidence that our optimized element effectively enhances the expression of EGFP and mCherry protein, and the protein expression levels are determined by the effectiveness of the AU-rich elements.

Next, to evaluate the potential of AU-rich elements in the context of antigen production, we used ovalbumin (OVA), a model antigen commonly used in immunological research and vaccine development due to its ability to stimulate robust immune responses. We constructed mRNAs encoding OVA Original, OVA-ARE-F, and OVA-ARE-T60, as depicted in Figure 4E. Western blot analysis of HeLa cells transfected with these constructs revealed significantly higher OVA production in the optimized OVA-ARE-F and OVA-ARE-T60 groups compared with the OVA Original group (Figure 4J). These results demonstrate that integrating AU-rich elements into the 3′ UTR can substantially enhance antigen production, suggesting its potential utility in mRNA vaccine development.

To assess the immunological effects of AU-rich element optimization, we encapsulated OVA-encoded mRNAs (OVA, OVA-ARE-F, and OVA-ARE-T60) into SM102 lipid nanoparticles (LNPs) and administered them intramuscularly to Balb/c mice on days 0 and 7, with 5 μg of mRNA per dose (Figure 4D). Serum samples were collected on days 4 and 12, and spleens were harvested on day 12 to analyze cellular and humoral immune responses.

Enzyme-linked immunosorbent spot (ELISpot) analysis revealed a significant increase in the interferon-gamma (IFN-γ)-producing cells in the spleens of mice vaccinated with OVA-ARE-F and OVA-ARE-T60, with the latter inducing approximately twice as many spots as OVA (Figures 4F and 4G). This finding indicates a robust antigen-specific cellular immune response. Consistent with this, enzyme-linked immunosorbent assay (ELISA) analysis of serum samples showed that OVA-ARE-T60 induced the highest levels of OVA-specific immunoglobulin (Ig)G antibodies, significantly surpassing the levels observed with OVA (Figures 4H, S5D, and S5E). These results highlight the potential of OVA-ARE-T60 to elicit strong systemic humoral immune responses, further supporting its use as a promising vaccine candidate.

Advances in RNA synthetic biology over the past few decades have highlighted the potential of various RNA elements to construct protein expression systems, which can perceive intracellular proteins and control translation. Building on the inspiration of RNA circuits, we

Table 2. Sequence of ARET10–T90 with optimal repeat length of AU-rich elements

Serial number	AU-rich sequence
ARE-T10	TATTTATTT
ARE-T30	ATTTATTTATTTATTTATTTATTTATTTA
ARE-T50	ATTTATTTATTTATTTATTTAATTTAT TTATTTATTTATTTATTTATTTA
ARE-T70	ATTTATTTATTTATTTATTTATTTATTTAT TTATTTATTTATTTATTTATTTATTTATTT ATTTATTTA
ARE-T90	ATTTATTTATTTATTTATTTATTTATTTATT TATTTATTTATTTATTTATTTATTTATTTAT TTATTTATTTATTTATTTATTTATTTA
ARE-T40	ATTTATTTATTTATTTATTTATT TATTTATTTATTTATTTA
ARE-T60	ATTTATTTATTTATTTATTTATTTATTTATT TATTTATTTATTTATTTATTTATTTATTTA

further co-transfected plasmids and RNA to overexpress the RNA-binding protein HuR (Figure 4I), increasing the protein levels of HuR and expanding the application potential of AU-rich elements. As shown in Figure 4K, western blot results demonstrate a significant increase in HuR protein expression after transfecting HuR plasmids and RNA compared with the control group. We co-transfected HuR plasmids and ARE-F RNA into cells to observe whether this could further increase protein output (Figure 4L). The results showed a notable rise in luciferase expression after co-transfection. In summary, the sequence optimization approach we proposed can draw from the ideas of RNA synthetic biology and could potentially initiate a novel type of RNA vaccine, like reverse-transcribed RNA vaccines[25,26] consisting of two RNA strands—one for expressing the target protein and the other for expressing a protein that enhances the expression of the target protein.

DISCUSSION

Although two mRNA-based COVID-19 vaccines have been introduced to the market, clinical trials have indicated that patients receiving high-dose mRNA vaccines experience more adverse events, which stem from lipid nanoparticles used in the vaccines. Therefore, improving mRNA translation efficiency and thus promoting its pharmacokinetics plays a crucial role in advancing mRNA technology. Our study introduces an approach to improve mRNA translation efficiency by incorporating sequences in the UTR that bind to cytoplasmic proteins. Furthermore, we demonstrate the functional significance of RNA-binding proteins in anchoring the inserted sequence, thereby regulating mRNA stability and translation. We also rationally designed the natural enhancer element and evaluated the effect of sequence changes of the elements on the production of synthetic mRNA.

Several cytoplasmic proteins can bind to AU-rich elements, among which HuR is one of the few proteins capable of stabilizing target RNA. In line with the previous research,[22,27,28] HuR plays a crucial role in improving RNA stability and translation through binding to AU-rich elements, which is in contrast to many RNA-binding proteins that accelerate RNA degradation. We creatively integrated AU-rich elements into the 3′ UTR to optimize the sequence, leveraging intracellular HuR as a stabilizing factor. From the perspective of synthetic mRNA drug development, the findings in this report provided enhanced UTR sequences for boosting the efficacy and reducing the dosage of synthetic mRNA therapeutics. We not only identified the optimal insertion location in 3′ UTR, but also demonstrated that enhancement effect of AU-rich elements is general: being independent of both encoded protein type and the type of transfected cell. This approach links the number of functional proteins to factors determining stability, presenting an optimization strategy grounded in a well-defined molecular mechanism. Our approach to enhancing mRNA stability diverges from a conventional high-throughput screening strategy on mRNA UTR sequences, which is often laborious and costly, and instead offers a novel rational design strategy for RNA sequence optimization.

We investigated the insertion of AU-rich elements into different positions within mRNA's 3′ UTR and found that compared with the middle or end of the 3′ UTR, insertion before the 3′ UTR led to the highest enhancement in protein expression. We speculate that the variation in enhancement is mainly due to changes in the secondary structure of the 3′ UTR. Complex structures may hinder the binding of HuR to AU-rich elements, especially when AU-rich elements are inserted into the middle or end of the 3′ UTR. These secondary structures may limit the efficiency of HuR binding to AU-rich elements, thereby weakening its enhancing effect on mRNA stability and translational efficiency. Additionally, multiple protein complexes can interact with mRNA within the 3′ UTR. When AU-rich elements are inserted before the 3′ UTR, there is less mutual interference between AU-rich elements and other proteins, allowing HuR to bind and form stable RNA-protein complexes more easily.

The stability and translation of mRNA are controlled by a complex network of RNA and protein interactions. Attribution of the potential positive role of HuR in the regulation of its target mRNA stability and translation is supported by the fact that the ARE-F luciferase level is lower when HuR activity is reduced, while the luciferase level of Non-ARE remains unchanged, implying that a constitutive HuR function facilitated this alteration. A plausible explanation is that the HuR protein competitively binds to the 3′ UTR, preventing translation suppression or degradation induced by unstable factors. These unstable factors mainly include RNase, RNA-binding proteins, and miRNA. Due to HuR's higher affinity for AU-rich elements, it selectively and preferentially binds to certain AU-rich elements, obstructing the binding of other post-transcriptional destabilizing factors simultaneously. This reduces the impact of destabilizing factors on mRNA degradation, ultimately enhancing mRNA stability and increasing protein expression.

Additionally, a deeper analysis of the binding patterns between HuR and AU-rich elements is essential. It is important to recognize that

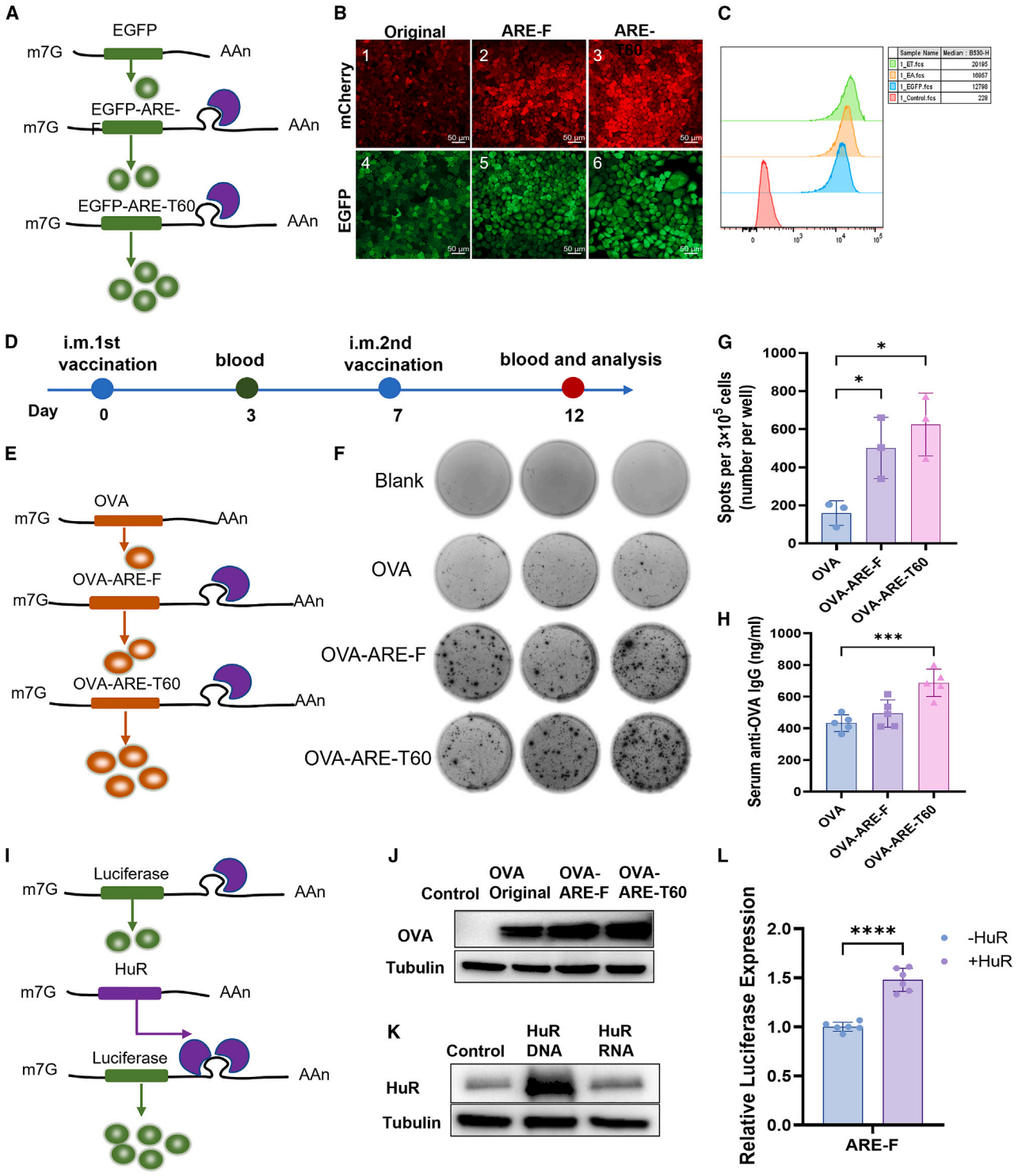

Figure 4. AU-rich elements as an optimization tool for various proteins

(A) Schematic representation of EGFP and optimized EGFP-ARE-F, EGFP-ARE-T60 RNA molecules. (B) Laser confocal microscopy detection of protein expression levels of EGFP Original and mCherry Original, as well as optimized EGFP-ARE-F, EGFP-ARE-T60, mCherry-ARE-F, and mCherry-ARE-T60 transfected cells after 24 h. (C) Flow cytometry showed the protein expression of EGFP (blue) and optimized EGFP-ARE-F (yellow), EGFP-ARE-T60 (green), and control (red) were blank cells without transfection,

(legend continued on next page)

not all AU-rich elements inserted into the 3′ UTR of mRNA can enhance translation. Despite the similarity in nucleotide sequences, with rich adenine and uridine bases, the minor differences in their sequences result in significant differences for RNA regulation. For instance, the protein expression levels of ARE-V6, ARE-V7, and ARE-T40 are notably lower, even two orders of magnitude lower than the expression levels of fluorescent proteins lacking AU-rich elements. This suggests that the RNA-binding proteins associated with these three AU-rich elements may facilitate RNA decay. RNA-binding proteins within cells exhibit different binding modes, affinities, and functions toward AU-rich elements.[29,30] Therefore, disparities in mRNA protein expression levels are likely attributed to alterations in a few nucleotides within AU-rich elements, which facilitate recruitment of RNA-binding proteins with varying functionalities. This emphasizes the importance of investigating these sequences in their interactions with diverse RNA-binding proteins.

In summary, we proposed a novel strategy to enhance mRNA stability and protein translation efficiency by introducing AU-rich elements in the 3′ UTR region of mRNA. The exact insertion location has been pinpointed at the beginning of the 3′ UTR for maximum protein expression. The protein responsible for subcellular binding to AU-rich elements is identified as HuR, as evidenced by pull-down assays and HuR knockdown experiments. Furthermore, we evaluated the translation efficiency of mRNA containing AU-rich elements with different repeats of core sequence and systematically redesigned the AU-rich sequences. We illustrated the functional significance of AU-rich elements in mRNA regulation both *in vitro* and *in vivo*, showcasing that AU-rich elements can serve as a universal tool for enhancing protein translation efficiency, thus expanding the potential applications of mRNA as both vaccines and therapeutics.

MATERIALS AND METHODS

Cell culture

A549, HeLa, HEK293T, NIH3T3, and DC2.4 cells were kindly provided by Cell Bank, Chinese Academy of Sciences. All cells were cultured at 37°C with 5% CO_2. All other cells were cultured in Dulbecco's modified Eagle's medium (DMEM) (Gibco) except DC2.4 with Roswell Park Memorial Institute (RPMI) medium 1640 basic (Gibco) supplemented with 10% fetal bovine serum (FBS) and antibiotic 1% penicillin/streptomycin.

dsDNA template generation

Templates for *in vitro* transcription were chemically synthesized (Genescript), located in the pUC57-Kana plasmid, and the reconstruction for the plasmids was done using a Q5 Site Directed Mutagenesis Kit (New England Biolabs) or Gibson assemble by pEASY-Basic Seamless Cloning and Assembly Kit (Transgene). All PCR reactions used the 2× Phanta Flash Master Mix Dye Plus (Vazyme). DNA templates include T7 promoter sequence, 5′ UTR fragment, open reading frame fragment, 3′ UTR fragment, and poly(A) tail sequence with 80 adenines in length. The 5′ UTR and 3′ UTR sequences have been reported in previous research and are available in Semantic Scholar (https://www.semanticscholar.org/paper/Assemblies-of-putative-SARS-CoV2-spike-encoding-for-Jeong-McCoy/150b70589516b969ce20fe83b9808478dd6f0e72). The plasmid was linearized by BspQI (New England Biolabs). The amounts of templates were determined by Nanodrop One (Themo Scientific). The purity of templates was assessed using agarose gel electrophoresis.

Synthesis and purification of mRNAs

Plasmids were linearized and mRNAs were synthesized using the T7 High Yield RNA Synthesis Kit (Hongene Biotech) that replaces uridine with N1-Me-Pseudo UTP (Hongene Biotech) and adds $m^7G(5')ppp(5')$ (2′-OMeA)pG solution (Hongene Biotech). The reaction mixtures were incubated at 37°C for 2 h and further incubated at 37°C for 30 min in the presence of DNase I (New England Biolabs). After *in vitro* transcription, mRNA purification was performed using the RNA Clean and Concentrator Kit (APExBIO), according to the manufacturer's protocol. The amounts of product mRNAs were determined by Nanodrop One (Themo Scientific). The purity of mRNAs was assessed using Qsep100 following the standard protocol using RNA Cartridge. mRNAs were diluted to 170 ng/μL in 50-mM citrate buffer (pH 4) for transfection and stored at −80°C until use.

Lipid-nanoparticle encapsulation of the mRNA and transfection

In brief, lipids were dissolved in ethanol containing an ionizable lipid SM102, 1, 2-distearoyl-sn-glycero-3-phosphocholine (DSPC, sinopes), cholesterol (sinopes), and methoxypoly(ethylene glycol) dimyristoylate (PEG-DMG-2K, sinopes) with a molar ratio of 50:10:37.5:2.5. The lipid mixture dissolved in the ethanol phase was combined with citrate buffer pH 4.0 containing mRNA at a ratio of 1:3 through a microfluidic device. For most experiments, 96-well plates were used. For mRNA stability, a six-well plate was used. Cells resuspended in DMEM plus 10% FBS were seeded ($1–1.5 \times 10^4$cells/well for a 96-well plate or $3–4.5 \times 10^5$cells/well for a six-well plate the night before the transfections. Typically, the amounts of mRNA transfected for 96-well plates and six-well plates are 127.5 ng and 5 μg, respectively. The transfection reagent and RNA solution were mixed and added to each well dropwise. The transfections were incubated at

cells ≥10,000. (D) Vaccination regimen administered to mice. (E) Schematic representation of OVA Original RNA and optimized OVA-ARE-F and OVA-ARE-T60 RNA molecules. (F) Optical images and (G) quantitative analysis of IFN-γ-spot-forming cells via ELISpot assay. Spleen cells of mice were plated and stimulated with an OVA peptide. (H) ELISA analysis of OVA protein-specific IgG levels in the serum from mice treated with OVA, OVA-ARE, and OVA-ARE-T60. (I) Schematic representation of increased transfection of HuR DNA molecules. (J) Western blot detection of OVA and protein expression levels of optimized OVA-ARE-F and OVA-ARE-T60 transfected cells after 24 h. (K) Western blot detection of increased cytoplasmic binding of AU-rich element HuR protein after transfection of HuR DNA and RNA. (L) Transfection of HuR plasmids increase cytoplasmic binding of AU-rich element HuR protein, further enhancing luciferase expression of ARE-F. $n \geq 3$. Data are presented as mean ± SD. Student's t test was used to evaluate significant differences: * $p < 0.05$, * * $p < 0.01$, * * * $p < 0.001$; NS, not significant.

37°C in 5% CO_2 for 6–48 h and the medium was replaced with DMEM plus 5% FBS.

Luciferase assay

After 24-h transfection with luciferase mRNA, the 96-well plate was removed to room temperature for 15 min. Then 100 μL of luciferase Assay Substrate (YEASEN) was added. The plate was gently shaken for 5–10 min in the dark. The supernatant of each well was transferred to a white 96-well plate (Themo Scientific). The bioluminescence was measured using a multimode microplate reader (TECAN Infinite E Plex).

qRT-PCR

Transfection was performed 24 h after seeding. HeLa cells at 3×10^5 cells/well were placed in a six-well plate. Five micrograms of luciferase mRNA was transfected into each well. The cell lysate was collected at different time points after the transfection, and total RNA was extracted using the Fast Pure Complex Tissue/Cell Total RNA Isolation Kit (Vazyme). The quality of total RNA was assessed using agarose gel electrophoresis. The amounts of RNA were determined by Nanodrop One (Themo Scientific). One microgram of total RNA was used to produce cDNA with gDNA Clean for qPCR (Accurate Biology) and 40 cycles using Premix Pro Taq HS qPCR Kit (Accurate Biology). All qPCR experimental steps are referenced to the instruction manual. The amount of intracellular luciferase mRNA was measured by the standard SYBR Green qRT-PCR protocol and amplification with luciferase and human glyceraldehyde-3-phosphate dehydrogenase (GAPDH) rRNA-specific primers. For luciferase mRNA, a forward primer: GTGTGATGACTCGAGCTGGT and a reverse primer: GTGTGGCTAGGCTAAGCGTT were used. For GAPDH mRNA, a forward primer: AATGGGCAGCCGTTAGGAAA and a reverse primer: GCCCAATACGACCAAATCAGAG were used. The qPCR analysis was performed using the LightCycler 480 Instrument II following the manufacturer's protocol with a three-step reaction. The Ct value from luciferase mRNA was normalized by the Ct value from GAPDH rRNA. All qPCRs were performed in technical duplicates and the averages of Ct were processed to calculate relative expression levels using the ΔΔCt method.

Western blot

Cells were lysed with high RIPA buffer (Solarbio), supplemented with protease inhibitor on ice for 15 min, and the supernatant was carefully transferred to a new centrifuge tube after being centrifuged at 12,000 × *g* for 10 min. Protein loading buffer was added to the supernatant. The sample was boiled for 10 min. The protein concentration was measured by BCA assay (Solarbio). An equal amount of total protein extract (30 mg) was separated by 4%–20% sodium dodecyl sulfate polyacrylamide gel electrophoresis (SDS-PAGE) at 140 V for 50 min. The samples were transferred to methanol-activated polyvinylidene fluoride (PVDF) membranes (Bio-Rad, CA, USA) using semi-dry transfer method by eBlot L1 Rapid Wet Transfer System (GenScript, L00686C). The membrane was blocked with 1 × TBST containing 5% skim milk for 1 h at room temperature, then incubated with primary antibody at 4°C overnight. The membranes were washed six times with 1 × TBST buffer per 5 min followed by incubation with secondary antibodies. At the end of incubation, the membranes were washed with 1 × TBST buffer six times, 5 min each. The protein was detected with ECL western blotting reagent and ChemiDoc XRS+. The exposure time was 30 s, the number of shots was 30, and the pictures of the film under natural light were taken for subsequent comparison of the molecular weight of the protein. The membranes were then imaged with β-tubulin following the above procedures. The images were analyzed with ImageJ densitometric measurements. The data are expressed as integrated density times area and presented as relative fold in comparison with corresponding control. Rabbit anti-HuR (Proteintech, CAT NO: 11910-1-AP) was used in 1:2,000 dilution.

siRNA transfection

The sequences of the siRNAs targeting HuR and control siRNA are as designed on Sangon Biotech. All siRNAs were transfected to HeLa cells at final concentration of 50 nM using Lipofectamine 3000 reagent (Themo Fisher Scientific) following the manufacturer's protocol. Cells transfected with siRNAs were harvested 48 h post-transfection.

siRNA sequences are listed below.

HuR siRNA sense 5′-3′(siHuR): GAGAACGAAUUUGAUCGUCA ATT.

NC siRNA sense 5′-3′(siNC): UUCUCCGAACGUGUCACGUTT.

Biotinylated RNA pull-down assays

Biotinylated RNA probes were synthetized on Genscript. RNA pull-down assay was performed according to the Pierce Magnetic RNA-Protein Pull-Down Kit (Themo Fisher Scientific). First, labeled RNA was bound to streptavidin magnetic beads. Fifty picomole biotin-labeled ARE-F RNA and negative RNA control (poly(A) RNA) was added to the beads, which were resuspended in capture buffer and incubated for 15–30 min at room temperature with agitation. The tube was placed into a magnetic stand to collect the beads, followed by washing the beads with an equal volume of 20 mM Tris (pH 7.5) and adding 100 μL of 1 × protein-RNA-binding buffer to the beads ready for binding cell lysate master mix. A 10-cm dish was prepared and lysed in a high lysis buffer. The 150 μL supernatant was collected, 20 μL of which was used as input. The remaining supernatant was divided into two parts and incubated with biotin-labeled ARE-F RNA probe streptavidin beads mixture or polyA RNA probe streptavidin beads mixture. The protein concentration of the cell lysate was determined by the BCA assay reagent. A 100-master mix of RNA-protein binding reaction containing 200 μg cell lysate, 30 μL 50% glycerol, 10 × protein-RNA-binding buffer, and nuclease-free water adjusted with the system. The master was mixed with the RNA-bound beads and incubated at 4°C for 60 min with agitation or rotation. The mixture was placed into the magnetic stand beads to collect the beads and washed with equal volume of one wash buffer three times. The bead-associated proteins were eluted by treating the beads with 50 μL 1 × SDS loading buffer for 15 min at 37°C followed by boiling with SDS-PAGE

loading buffer for 5 min. The eluted proteins were analyzed by western blotting.

Immunofluorescence

Briefly, cells were rinsed twice in PBS, fixed in 4% paraformaldehyde fix solution (Beyotime), and permeabilized with 0.5% Triton X-100. After permeabilization, cells were blocked for 60 min and after being incubated with primary antibodies against the RNA-binding proteins HuR (1:2,000) and at room temperature for 1 h or at 4°C overnight. The cells were then incubated with goat anti-rabbit secondary antibodies (Proteintech CoraLite488-conjugated,1:500) and stained with DAPI (4,6-diamidino-2-phenylindole) to visualize the nucleus. A Zeiss LSM980 confocal microscope was used to observe the cells using a 40× oil objective, and a (Zeiss) digital camera was used for immunofluorescence photography.

In vivo bioluminescence

This study was reviewed and approved by the Biomedical and Medical Ethics Committee of Dalian University of Technology (Approval No. DUTSEB20228-08). For *in vivo* studies, 6- to 8-week-old female BALB/c mice (Changsheng biotechnology co., Ltd.) were maintained under specific-pathogen-free conditions and were kept with a 12 h/12 h light/dark cycle in individually ventilated cages, provided with food and water ad libitum. All animal procedures were approved and controlled by the local ethics committee and carried out according to the guidelines of protection of animal life. Vaccines were administered via subcutaneous injection to the mice. The injection site was located at the back of the mouse's neck. Prior to injection, the back and neck of the mice were depilated to prevent hair from interfering with the imaging signals and were disinfected with 70% ethanol prior to administration to minimize the risk of infection. Before subcutaneous administration, the encapsulation efficiency was determined using the Quant-iT RiboGreen RNA Reagent and Kit (Thermo Fisher Scientific). Each mouse was injected with 5 μg of RNA. At 6, 24, and 48 h after mRNA injection,[31] the mice were anesthetized intraperitoneally with Isoflurane and injected intraperitoneally with D-Luciferin solution (150 mg/kg mice). The bioluminescent images of the mice were taken 10 min after D-Luciferin injection on an *in vivo* imaging system. The total bioluminescence signals of the abdomen were recorded for calculation.

Microscope imaging

For the imaging of HeLa cells, cells were seeded in a 35-mm confocal culture dish at a density of 1×10^5 cells per well. After 24 h, transfecting with EGFP original, EGFP-ARE-F, EGFP-ARE-T60 mRNA, mCherry original, mCherry-ARE-F, mCherry-ARE-T60 mRNA, the amount of mRNA transfected into each dish is 5 μg. Before imaging, the culture medium was removed and washed three times using 1× PBS. Cells were imaged in PBS buffer at the end. Fluorescence images of transfected cells were acquired with appropriate excitation light and filter cubes used a Zeiss LSM980 confocal microscope: all imaging was performed using a 20× objective. For EGFP fluorescence imaging, an excitation wavelength of 488 nm and an emission wavelength of 509 nm were utilized. For mCherry fluorescence imaging, an excitation wavelength of 587 nm and an emission wavelength of 610 nm were employed.

Flow cytometry analysis

We analyzed fluorescent protein expression by flow cytometry. Cells were prepared in six-well plates at a density of 3×10^5 cells per well and transfected the following day. After 48-h transfection, cells were harvested using 0.25% EDTA-Trypsin and resuspended in 200 μL cold 1% PBS solution. Cells were then transferred to a microcentrifuge tube and kept on ice. All the cells were analyzed using a BECKMAN CytoFlexs. A total of 10,000 cells were analyzed for each sample. For flow cytometric analysis to detect EGFP, a 488-nm excitation laser and B 525/30 nm filter were used. To detect mCherry, we used a 488-nm excitation laser and a Red-B 610/50 nm filter. Dead cells and debris were removed by front and lateral light scattering signals, and doublet discrimination was performed by area and height of front scattering signals. A negative control sample was transfected with only the LNP. To quantify EGFP protein expression, media fluorescence intensities were presented for comparison. The median EGFP fluorescence intensity from the positively transfected cell population was then compared with the intensity of EGFP mRNA carrying an AU-rich element that had been optimized for insertion.

ELISpot and ELISA analysis

Balb/c mice (6–8 weeks old) were intramuscularly injected with 5 μg of mRNA-LNP vaccines (OVA Original, OVA-ARE-F, or OVA-ARE-T60) on days 0 and 7. Blood samples were collected on days 4 and 12, and spleens were harvested on day 12 for immune analysis. The OVA-specific, IFN-γ-producing cells in the spleen were analyzed by ELISpot. The single-cell suspension of the spleen was prepared first. The ELISpot plates were coated with IFN-γ-specific antibodies (MabTech, Cat. 3321-4APW-2), washed with PBS, and blocked with culture medium for 4 h. Then, 3×10^5 of spleen cells were added to each well and stimulated with 5 μg/mL OVA peptide for 24 h. Spots were visualized with biotin-conjugated anti-IFN-γ antibody followed by incubation with streptavidin-alkaline phosphatase and BCIP/NBT substrate. The number of spots per well were counted by eye using an MabTech ELISpot reader.

The OVA-specific total IgG and OVA protein in serum were analyzed by ELISA (COIBO BIO, Cat. CB10499-Mu, CB11655-Mu). Briefly, 50 μL of serum and 100 μL of enzyme conjugate were added to wells and incubated for 60 min at 37°C. The microtiter plate was washed four times. Fifty microliters each of Substrate A and Substrate B was added to each well, gently mixed, and incubated for 15 min at 37°C. Fifty microliters of stop solution was added and the optical density (O.D.) was read at 450 nm using a microtiter plate reader within 15 min.

Quantification and statistical analysis

Statistical values including the exact N and statistical significance are reported in the figure legends. Standard deviation was calculated

using Excel. Significant differences were determined using one-way ANOVA. The statistical analysis is based on the means generated from at least three independent experiments, unless specified otherwise. Dot plots and histograms were produced from Invitrogen Attune NxT flow cytometry software. The levels of significance are denoted as $^{*}p < 0.05$, $^{**}p < 0.01$, $^{***}p < 0.001$.

DATA AVAILABILITY

The data supporting this study's findings are available from the corresponding author upon reasonable request.

ACKNOWLEDGMENTS

The authors would like to express their gratitude for the generosity of technicians in Dalian University of Technology Instrument Sharing Platform. The authors would like to acknowledge the valuable suggestions made by Dr. Liuwei Zhang. We also thank the Proxybio Therapeutics company for their generous gift of EGFP, mCherry, OVA plasmid, and the nucleotide raw material from Glycogene company. The work is supported by the National Key Research and Development Program of China (2023YFC3405000 to L.M.), Beijing Natural Science Foundation (Z220022, to L.M.), Beijing Municipal Science & Technology Commission (Z231100007223012 to L.M.), the National Natural Science Foundation of China (NSFC) grants (HY2021-8, 82373807 to L.M.), and Liaoning Provincial Science and Technology Program Joint Fund (2023JH2/101700343).

AUTHOR CONTRIBUTIONS

All authors reviewed and provided substantive input during the preparation of the manuscript. J.L. and X.M. designed the research. X.M. executed the experiments and analyzed the result. S.L. and B.F. assisted in plasmid construction experiments. S.L. and B.F. assisted with the data collection and validated the result. D.J. assisted in animal experiments. L.L., S.D., and J.L assisted with RNA characterization and data curation. J.L., S.D., and X.M. wrote the manuscript. L.M. coordinated and supervised the project. All authors have read and approved the manuscript and its content.

DECLARATION OF INTERESTS

The authors declare no competing interests.

SUPPLEMENTAL INFORMATION

Supplemental information can be found online at https://doi.org/10.1016/j.omtn.2025.102485.

REFERENCES

1. Baden, L.R., El Sahly, H.M., Essink, B., Kotloff, K., Frey, S., Novak, R., Diemert, D., Spector, S.A., Rouphael, N., Creech, C.B., et al. (2021). Efficacy and Safety of the mRNA-1273 SARS-CoV-2 Vaccine. N. Engl. J. Med. *384*, 403–416.
2. Sergeeva, O.V., Koteliansky, V.E., and Zatsepin, T.S. (2016). mRNA-based therapeutics–Advances and perspectives. Biochemistry *81*, 709–722.
3. Garneau, N.L., Wilusz, J., and Wilusz, C.J. (2007). The highways and byways of mRNA decay. Nat. Rev. Mol. Cell Biol. *8*, 113–126.
4. Wu, X., Shan, K.J., Zan, F., Tang, X., Qian, Z., and Lu, J. (2023). Optimization and Deoptimization of Codons in SARS-CoV-2 and Related Implications for Vaccine Development. Adv. Sci. *10*, 2205445.
5. Gebre, M.S., Rauch, S., Roth, N., Yu, J., Chandrashekar, A., Mercado, N.B., He, X., Liu, J., McMahan, K., Martinot, A., et al. (2022). Optimization of non-coding regions for a non-modified mRNA COVID-19 vaccine. Nature *601*, 410–414.
6. Holtkamp, S., Kreiter, S., Selmi, A., Simon, P., Koslowski, M., Huber, C., Türeci, O., and Sahin, U. (2006). Modification of antigen-encoding RNA increases stability, translational efficacy, and T-cell stimulatory capacity of dendritic cells. Blood *108*, 4009–4017.
7. Linares-Fernández, S., Moreno, J., Lambert, E., Mercier-Gouy, P., Vachez, L., Verrier, B., and Exposito, J.-Y. (2021). Combining an optimized mRNA template with a double purification process allows strong expression of *in vitro* transcribed mRNA. Mol. Ther. Nucleic Acids *26*, 945–956.
8. Cao, J., Novoa, E.M., Zhang, Z., Chen, W.C.W., Liu, D., Choi, G.C.G., Wong, A.S.L., Wehrspaun, C., Kellis, M., and Lu, T.K. (2021). High-throughput 5′ UTR engineering for enhanced protein production in non-viral gene therapies. Nat. Commun. *12*, 4138.
9. Orlandini Von Niessen, A.G., Poleganov, M.A., Rechner, C., Plaschke, A., Kranz, L.M., Fesser, S., Diken, M., Löwer, M., Vallazza, B., Beissert, T., et al. (2019). Improving mRNA-Based Therapeutic Gene Delivery by Expression-Augmenting 3′ UTRs Identified by Cellular Library Screening. Mol. Ther. *27*, 824–836.
10. Kirshina, A., Vasileva, O., Kunyk, D., Seregina, K., Muslimov, A., Ivanov, R., and Reshetnikov, V. (2023). Effects of Combinations of Untranslated-Region Sequences on Translation of mRNA. Biomolecules *13*, 1677.
11. Zhang, H., Zhang, L., Lin, A., Xu, C., Li, Z., Liu, K., Liu, B., Ma, X., Zhao, F., Jiang, H., et al. (2023). Algorithm for Optimized mRNA Design Improves Stability and Immunogenicity. Nature *621*, 396–403.
12. Castillo-Hair, S.M., and Seelig, G. (2022). Machine Learning for Designing Next-Generation mRNA Therapeutics. Acc. Chem. Res. *55*, 24–34.
13. Chan, J.J., Tabatabaeian, H., and Tay, Y. (2023). 3′UTR heterogeneity and cancer progression. Trends Cell Biol. *33*, 568–582.
14. Tian, B., and Manley, J.L. (2017). Alternative polyadenylation of mRNA precursors. Nat. Rev. Mol. Cell Biol. *18*, 18–30.
15. Jiang, Y., Xu, X.-S., and Russell, J.E. (2006). A Nucleolin-Binding 3′ Untranslated Region Element Stabilizes β-Globin mRNA In Vivo. Mol. Cell Biol. *26*, 2419–2429.
16. Sánchez, B.J., Mubaid, S., Busque, S., de los Santos, Y.L., Ashour, K., Sadek, J., Lian, X.J., Khattak, S., Di Marco, S., and Gallouzi, I.-E. (2023). The formation of HuR/YB1 complex is required for the stabilization of target mRNA to promote myogenesis. Nucleic Acids Res. *51*, 1375–1392.
17. Karmouch, J., Delers, P., Semprez, F., Soyed, N., Areias, J., Bélanger, G., Ravel-Chapuis, A., Dobbertin, A., Jasmin, B.J., and Legay, C. (2020). AChR β-Subunit mRNAs Are Stabilized by HuR in a Mouse Model of Congenital Myasthenic Syndrome With Acetylcholinesterase Deficiency. Front. Mol. Neurosci. *13*, 568171.
18. Siang, D.T.C., Lim, Y.C., Kyaw, A.M.M., Win, K.N., Chia, S.Y., Degirmenci, U., Hu, X., Tan, B.C., Walet, A.C.E., Sun, L., and Xu, D. (2020). The RNA-binding protein HuR is a negative regulator in adipogenesis. Nat. Commun. *11*, 213.
19. Siegel, D.A., Le Tonqueze, O., Biton, A., Zaitlen, N., and Erle, D.J. (2022). Massively parallel analysis of human 3′ UTRs reveals that AU-rich element length and registration predict mRNA destabilization. G3 (Bethesda) *12*, jkab404.
20. Chen, C.Y., and Shyu, A.B. (1994). Selective degradation of early-response-gene mRNAs: functional analyses of sequence features of the AU-rich elements. Mol. Cell Biol. *14*, 8471–8482.
21. Dreher, T.W. (1999). Functions of the 3′-Untranslated Regions of Positive-Strand RNA Viral Genomes. Annu. Rev. Phytopathol. *37*, 151–174.
22. Fan, X.C., and Steitz, J.A. (1998). Overexpression of HuR, a nuclear-cytoplasmic shuttling protein, increases the *in vivo* stability of ARE-containing mRNAs. EMBO J. *17*, 3448–3460.
23. Vogel, A.B., Kanevsky, I., Che, Y., Swanson, K.A., Muik, A., Vormehr, M., Kranz, L.M., Walzer, K.C., Hein, S., Güler, A., et al. (2021). BNT162b vaccines protect rhesus macaques from SARS-CoV-2. Nature *592*, 283–289.
24. Xia, X. (2021). Detailed Dissection and Critical Evaluation of the Pfizer/BioNTech and Moderna mRNA Vaccines. Vaccines *9*, 734.
25. Schmidt, C., Hastert, F.D., Gerbeth, J., Beissert, T., Sahin, U., Perkovic, M., and Schnierle, B.S. (2022). A Bivalent Trans-Amplifying RNA Vaccine Candidate Induces Potent Chikungunya and Ross River Virus Specific Immune Responses. Vaccines *10*, 1374.
26. McKay, P.F., Hu, K., Blakney, A.K., Samnuan, K., Brown, J.C., Penn, R., Zhou, J., Bouton, C.R., Rogers, P., Polra, K., et al. (2020). Self-amplifying RNA SARS-CoV-2 lipid nanoparticle vaccine candidate induces high neutralizing antibody titers in mice. Nat. Commun. *11*, 3523.
27. Otsuka, H., Fukao, A., Funakami, Y., Duncan, K.E., and Fujiwara, T. (2019). Emerging Evidence of Translational Control by AU-Rich Element-Binding Proteins. Front. Genet. *10*, 332.

28. Sidali, A., Teotia, V., Solaiman, N.S., Bashir, N., Kanagaraj, R., Murphy, J.J., and Surendranath, K. (2021). AU-Rich Element RNA Binding Proteins: At the Crossroads of Post-Transcriptional Regulation and Genome Integrity. Int. J. Mol. Sci. *23*, 96.

29. Dolicka, D., Sobolewski, C., Correia de Sousa, M., Gjorgjieva, M., and Foti, M. (2020). mRNA Post-Transcriptional Regulation by AU-Rich Element-Binding Proteins in Liver Inflammation and Cancer. Int. J. Mol. Sci. *21*, 6648.

30. Moore, K.S., and von Lindern, M. (2018). RNA Binding Proteins and Regulation of mRNA Translation in Erythropoiesis. Front. Physiol. *9*, 910.

31. Li, C.Y., Liang, Z., Hu, Y., Zhang, H., Setiasabda, K.D., Li, J., Ma, S., Xia, X., and Kuang, Y. (2022). Cytidine-containing tails robustly enhance and prolong protein production of synthetic mRNA in cell and *in vivo*. Mol. Ther. Nucleic Acids *30*, 300–310.